Dalton Transactions

ROYAL SOCIETY OF CHEMISTRY

FRONTIER

View Article Online
View Journal | View Issue

Cite this: *Dalton Trans.*, 2024, **53**, 15782

Colour/luminescence changes of transition metal complexes induced by gaseous small molecules for monitoring reaction progress and environmental changes

Kazuteru Shinozaki

Received 24th June 2024,
Accepted 4th August 2024

DOI: 10.1039/d4dt01822b

rsc.li/dalton

Transition metal complexes act as monitoring devices for reaction progress and environmental changes through their color/luminescence changes. In this paper, we focus on colour/luminescence changes induced by gaseous small molecules in the environment. The gradual decrease in O_2 content in solution can be monitored by the luminescence enhancement of an Ir(III) complex in dimethyl sulfoxide during photoirradiation. CO_2 in air can be captured by a Pt(II) complex in basic aqueous solution, resulting in a colour change from yellow to red to blue-green due to higher degree aggregate formation. Moisture in air induces colour/luminescence changes in Ru(II) and Ir(III) complex salts due to the sorption of H_2O into hydrophilic channels in the crystal. Volatile organic compound vapours such as $CHCl_3$ and CH_2Cl_2 change the purple colour of Pt(II) complex crystals to red and blue, respectively. The purple crystal can adsorb two $CHCl_3$ molecules under ambient conditions but only one CH_2Cl_2 molecule.

Introduction

Transition metal complexes (TMCs) showing strong luminescence and intense colour have attracted great attention from researchers involved in luminescence/colour studies across many fields including chemistry, biology, materials science, *etc.*, because of their applications in synthesis, catalysis, sensors, bio-imaging, and OLEDs. The colour and luminescence occasionally change upon exposure to small amounts of gaseous molecules such as O_2, CO_2, H_2O, or volatile organic compounds (VOCs). These characteristic responses to gaseous molecules are useful for the fabrication of monitoring devices for reactive and toxic chemicals based on emission measurements with quick response and high sensitivity. For example, phosphorescence from an excited TMC is quenched by O_2 to produce reactive oxygen species ($^1O_2$), which selectively attacks and kills cancer cells in photodynamic therapy (PDT).[1] However, in aerated dimethyl sulfoxide (DMSO) solution, phosphorescence is enhanced rather than quenched, where O_2 contributes not to phosphorescence quenching but to the oxidation reaction of the DMSO molecule.[2] Another example is the colour change resulting from the CO_2 insertion reaction of M–OH to M–CO_3H,[3] which proceeds spontaneously under ambient conditions, capturing CO_2 from the air along with a remarkable colour change. Vapochromism is the most characteristic phenomenon of TMCs involved in colour and luminescence changes induced by gaseous small molecules.[4] Some salts consisting of TMCs and counterions contain waters of crystallization, which are easily lost upon heating accompanied by a crystal colour change. Since the heated crystal retains its intrinsic crystal framework, the original crystal colour can be recovered by the sorption of H_2O molecules upon exposure to moisture in the air. Additionally, exposure to VOCs can trigger colour/luminescence changes in the Pt(II) complex crystal. The quick response and high sensitivity in vapochromism are useful for monitoring environmental changes in our daily lives; for example, the Pt(II) complex crystal can provide an alert signal through colour/luminescence changes when VOCs are emitted from household products.[4a,5]

In this manuscript, we summarize our recent studies on the colour/luminescence changes of TMCs as monitoring devices for reaction progress and environmental changes in the following sections.

Emergence of NIR absorption by higher degree aggregate formation of the Pt(II) complex due to the capture of CO_2 [6]

CO_2 capture and storage (CCS) is an important concept for achieving net-zero emissions and realizing a sustainable

Graduate School of Nanobioscience, Yokohama City University, 22-2 Seto, Kanazawa-ku, Yokohama 236-0027, Japan. E-mail: shino@yokohama-cu.ac.jp

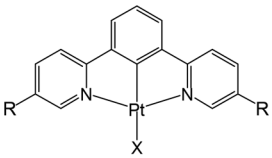

Fig. 1 Structure of **1** (R = COOH and X = OH^-) and **2** (R = COO^- and X = CO_3^{2-}).

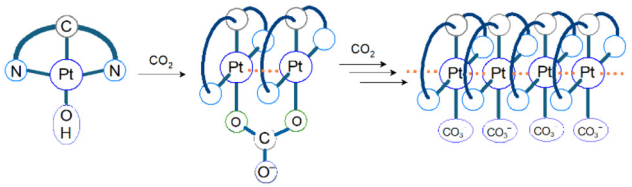

Fig. 2 An image of aggregation resulting from the reaction of complex **1** with CO_2 in basic aqueous solution. The CO_2 gas bubbling causes the aggregate formation. The degree of aggregation increases up to at least 32.

society. Since the concentration of CO_2 in the air is as low as 0.04%, the development of effective methods to capture CO_2 from the air is highly desirable. The CO_2 insertion reaction using TMCs offers an advantage for CCS because we can easily monitor the progress of the reaction through colour changes in response to CO_2 insertion. The CO_2 insertion induces aggregate formation in Pt(II) complex **1** (Fig. 1), accompanied by a colour change in aqueous solution from yellow to blue-green. The blue-green colour results from strong and broad absorption bands of the aggregate in the visible–near infrared (NIR) region assigned to the metal-to-ligand charge-transfer (MMLCT) transition. Recrystallization of **1** from sodium carbonate aqueous solution (Na_2CO_3 aq) provides both red and blue-green polymorphic crystals. The red colour of one of the polymorphs originates from the MMLCT transition of the Pt–Pt stacked dimer, where Pt(II) complex monomers are bridged by CO_3^{2-} ions. For the blue-green colour of the other crystal, although X-ray crystallography has not yet succeeded, it is known that the crystal is constructed from arrays of complex **2** (–Pt–Pt–Pt–) connected by Pt–Pt interactions (Fig. 2). The formation process of the blue-green aggregate in the aqueous solution was monitored through transient absorption spectroscopy. A global analysis of the spectral changes provided evidence for the formation of a 32-mer of complex **2** in the blue-green solution.

Emission enhancement of *fac*-[Ir(ppy)$_3$] (ppyH = 2-phenylprydine) by consuming O_2 in DMSO[7]

The phosphorescence of TMCs, such as *fac*-[Ir(ppy)$_3$], consisting of heavy atoms is often quenched by O_2 due to efficient triplet–triplet energy transfer, producing a strong oxidant, $^1O_2$. Therefore, the photosensitization of phosphorescent TMCs has been applied in photodynamic therapy (PDT) for killing cancer cells and in new synthetic procedures involving oxidation reactions using reactive oxygen.[10,11] Dimethyl sulfoxide (DMSO) has been widely used as a solvent in organic syntheses and PDTs because of its low toxicity, high polarity, and capability of dissolving many compounds. In aerated DMSO, photoirradiation gradually enhances the emission intensity of *fac*-[Ir(ppy)$_3$] due to the prevention of quenching by O_2, and the resultant intense-emission is suddenly quenched upon shaking the solution.[2] The suppression of quenching during the photoirradiation is reasonably accounted for by the consumption of $^3O_2$ through the formation of dimethyl sulfone (DMS) in the photosensitized reaction involving *fac*-[Ir(ppy)$_3$]* and the ^{3}(O_2-DMSO) adduct. Since $^3O_2$ rapidly reacts with DMSO under ambient conditions when $^3O_2$ is dissolved in DMSO, photosensitization of *fac*-[Ir(ppy)$_3$] potentially contributes to the activation of ^{3}(O_2-DMSO) to labile ^{1}(O_2-DMSO) rather than $^3O_2$ to $^1O_2$. The sudden drop in emission intensity upon shaking is accounted for by quenching from ^{3}(O_2-DMSO) formed from fresh $^3O_2$ dissolved in the solution from the air or gas phase in the cuvette. DFT calculations supported that the formation of ^{1}(O_2-DMSO) is energetically more favourable than the formation of $^1O_2$. We clarified the mechanism of a series of photochemical reactions in this system through kinetic analysis of DMS production along with the emission enhancement of *fac*-[Ir(ppy)$_3$]. This analysis reproduced not only the production process of DMS but also the production/consumption processes of all species involved in the photosensitization, including transient *fac*-[Ir(ppy)$_3$]* and ^{1}(O_2-DMSO). This DMS production *via* photosensitization can continue until all the $^3O_2$ in the DMSO solution is completely consumed. It should be noted that the ^{1}(O_2-DMSO) adduct could participate in substrate oxidation in organic syntheses and in killing cells due to photosensitization using DMSO as a solvent (Scheme 1).

Detection of H_2O through colour changes in TMC salt crystals[8]

TMC salts can detect moisture through changes in crystal colour in response to the sorption/desorption of H_2O molecules into/from the crystal. For the demonstration of this vapochromic performance, it is required that the crystal exhibits a remarkable colour change upon attachment/detachment of H_2O, possesses a robust crystal framework for the sorption/desorption cycle of H_2O molecules, and has channels through which H_2O molecules can move. For the crystal of *fac*-[Ir(tpy)$_2$]I_3·$2H_2O$ (tpy = 2,2′:6′,2″-terpyridine), a reversible colour change

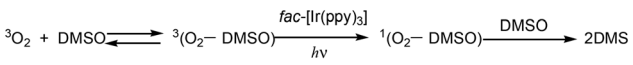

Scheme 1 Reaction of O_2 consumption by photosensitization of *fac*-[Ir(ppy)$_3$].

between red and orange is observed in response to heating and cooling cycles. Since both intense colours originate from the I^--to-ligand charge-transfer (XLCT) transition, the colour change can be accounted for by the difference in the interaction between I^- and the tpy ligand, resulting from the attachment/detachment of H_2O to/from I^-, respectively. Single crystal X-ray crystallography clarified that the Ir(III) complex possesses I^- ions at distances of 2.9–3.1 Å from the closest H atoms of the tpy ligand, suggesting that the XLCT transition results from the interaction between the I^- 5p orbital and tpy π^* orbital. The two waters of crystallization, involved in the vapochromism, form a dimer structure, $r_{O\text{–}O}$ = 2.911 Å, by hydrogen bonding. The H_2O dimer connects to one of the $^-$ ions with $r_{O\text{–}I}$ = 3.664 Å by hydrogen bonding and contacts another I^- ion with $r_{O\text{–}I}$ = 3.747 Å, suggesting that the XLCT transition is easily changed by H_2O desorption from the crystal. Thermogravimetric (TG) measurements revealed step-by-step H_2O desorption from the crystal, and powder X-ray diffraction (PXRD) showed the robustness of the Ir(III) complex crystal framework during the sorption/desorption cycles. The H_2O desorption takes place even at room temperature upon blowing dry nitrogen gas or exposure to organic solvent vapour, which results in a red coloration of the crystal. Conversely, when the red crystal of $[Ir(tpy)_2]I_3$ is exposed to H_2O vapour, the crystal colour returns to orange even at ambient temperature. It is suggested that the hydrogen bonding of H_2O to I^- is too weak to keep H_2O molecules in the vicinity of I^-.

$M[Ru(bpy)(CN)_4]$ (M^{2+} = Ca^{2+} or Sr^{2+}) acts as a moisture sensing device showing reversible colour and luminescence changes; both emission spectra of Ca^{2+} and Sr^{2+} salts are remarkably shifted to the longer wavelength region with increasing temperature from 296 to 500 K. An X-ray crystallographic study revealed that the crystals are constructed from linear chains of $\{[Ru(bpy)(CN)_4][Ca(H_2O)_5]\}_n$ and $\{[Ru(bpy)(CN)_4][Sr(H_2O)_6]\}_n$. The chain –Ru–CN–$M^{2+}$–NC–Ru– (Fig. 3) guarantees the robustness of the crystal during the sorption/desorption cycles of H_2O. The hydrophilic channels between these chains contribute to the sorption/desorption of H_2O into/from the crystal. Changes in the interaction of the M^{2+} ion with the equatorial CN ligand, depending on the number of H_2O molecules attached to the M^{2+} ion, effectively contribute to colour/luminescence changes in the Ca^{2+} and Sr^{2+} salts. The results of TG measurements indicated that heating above 470 K enables the desorption of five H_2O molecules for both salts, resulting in $\{[Ru(bpy)(CN)_4][Ca]\}_n$ and $\{[Ru(bpy)(CN)_4][Sr(H_2O)]\}_n$. The changes in the hydration structure around the M^{2+} ion regulate the shift of CN stretching modes, leading to a redshift in the ruthenium-to-bpy CT (MLCT) excited state. It should be noted that the colour/luminescence changes are caused by the changes in the MLCT transition energy modulated by the attachment/detachment of H_2O to the M^{2+} ion but not the Ru(II) complex ion. The luminescence change based on the weak interaction between the M^{2+} ion and the CN ligand of Ru(II) complexes provides a novel design guideline for vapochromic materials.

Colour changes of the crystal upon exposure to halomethane vapour and selective sensing of $CHCl_3$ [9]

Pt(II) complex **3** (Fig. 4) is obtained as a red precipitate from $CHCl_3$. However, surprisingly, when this precipitate is collected by suction filtration, the resultant material's colour rapidly changes to purple, and conversely, the purple colour changes to red upon exposure to $CHCl_3$ vapour. The reversible colour-change between purple and red is accounted for by the vapochromic response of crystal **3** to $CHCl_3$ vapour. Since the red and purple crystals emit red and NIR luminescence, respectively, we can perceive the vapochromism as an ON/OFF switch for red emission during the evacuation and exposure cycles of $CHCl_3$ vapour. These characteristic features promise quick and highly sensitive detection of small amounts of $CHCl_3$ vapour using crystal **3**. X-ray crystallography of the red form revealed that two Pt(II) complexes are mutually twisted by *ca.* 180°, resulting in a head-to-tail arrangement of stacked dimers and the Pt–Pt units are aligned along the *b*-axis of the unit cell, forming infinite columnar structures. The $CHCl_3$ molecules are stored in channels between these infinite –Pt–Pt–Pt– columns and thereby are desorption/sorption through the channels from/into the crystal. During the exposure to $CHCl_3$ vapour, a step-by-step change from **3** to **3**·$CHCl_3$ to **3**·2$CHCl_3$ was observed. Unlike the $M[Ru(bpy)(CN)_4]$ and $[Ir(tpy)_2]I_3$ systems, the peak patterns in PXRD obtained for the crystals are different from one another, suggesting that the crystal framework consisting of complex **3** is soft and easily altered during the sorption/desorption cycles of $CHCl_3$. When purple crystal **3** is exposed to CH_2Cl_2 vapour, which is chemically very similar to $CHCl_3$, the colour of the crystal changes to blue (Fig. 5). This behaviour suggests that crystal **3** has the capability to discriminate $CHCl_3$ from chemically similar CH_2Cl_2. A change in the PXRD pattern of crystal **3** upon increasing the CH_2Cl_2 vapour pressure up to 50 kPa showed a

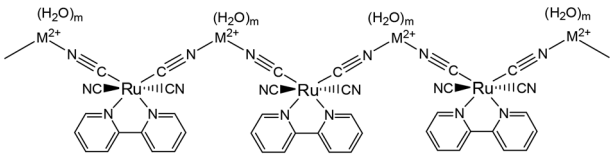

Fig. 3 Chain structure of $\{[Ru(bpy)(CN)_4][M(H_2O)_m]\}_n$. The number of H_2O (m) depends on temperature.

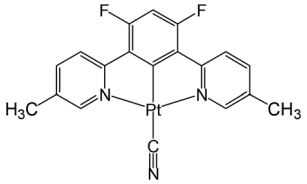

Fig. 4 Structure of complex **3**.

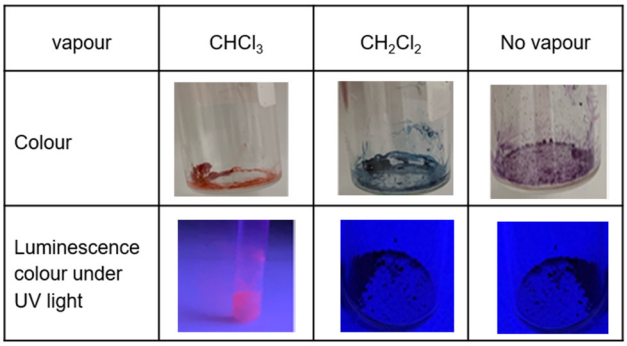

Fig. 5 Colour and luminescence variations of complex **3** in the solid state. (Top) The purple crystal of complex **3** changes to red and blue upon exposure to $CHCl_3$ and CH_2Cl_2 vapours, respectively. (Bottom) The red crystal containing $CHCl_3$ emits red luminescence, whereas both blue and purple crystals emit invisible NIR luminescence. This figure has been reproduced from ref. 8 with permission from the Royal Society of Chemistry, copyright 2022.

two-step peak change due to the sorption of CH_2Cl_2 similar to when exposed to $CHCl_3$ vapour. Therefore, the difference between $CHCl_3$ and CH_2Cl_2 in the vapochromic behaviour of crystal **3** under ambient conditions is concluded to be due to the difference in the number of molecules in the crystal; the purple crystal **3** can adsorb two $CHCl_3$ molecules under ambient conditions but just one CH_2Cl_2 molecule (Fig. 5).

Conclusion

We presented changes in the colour/luminescence of TMCs induced by small molecules, enabling the visualization of the progress of chemical reactions involving these small molecules and changes in the surrounding atmosphere. A water-soluble Pt(II) complex reacts with CO_2, resulting in higher degree aggregate formation and showing broad absorption across the visible to NIR region. Although we estimate that the degree of aggregation increases up to 32, the structure of the aggregate remains unknown. Recently, to identify the structure and morphology of the supramolecular assembly of Pt(II) complexes, measurements of circularly polarized luminescence have been conducted.[4b] However, studies on the structure of supramolecular assemblies or aggregates of Pt(II) complexes are still limited. We showed that the enhancement/quenching of emission from *fac*-[Ir(ppy)$_3$] can be used in a monitoring device for tracking the progress of desired reactions in PDT. Moreover, we found that the O_2-DMSO adduct contributes to the catalytic formation of DMS by excited *fac*-[Ir(ppy)$_3$]. Therefore, further investigation into the O_2-DMSO adduct should be performed for understanding the fundamental photodynamic effects of TMC phosphors dissolved in DMSO. For TMC salt crystals, the robustness of the crystal framework and the presence of hydrophilic channels are significant for repeatable sorption/desorption cycles of H_2O, and the reversible colour/luminescence changes result from the indirect interaction of H_2O with the TMC and the weak bonding of H_2O to the counterion. We should clarify and understand the photophysics of the indirect interactions contributing to the colour/luminescence changes of TMCs. For molecular crystals of Pt(II) complexes, the "softness" of the crystal is important for vapochromism; the Pt(II) complex easily changes the intermolecular arrangement and Pt–Pt distance responsible for the coloration of the crystal. Although substantial knowledge on changes in the crystal structure upon applying mechanical stress or grinding has been accumulated,[4c] further investigation into the "softness" of the crystal is needed to clarify and understand the vapochromism of Pt(II) complexes. Since the Pt(II) complex crystal can discriminate $CHCl_3$ from CH_2Cl_2, it is expected to be a detection device for specific molecules in a variety of VOCs. This may contribute to further improvements in sensors for VOCs and toxic chemicals using TMCs.[4a] It is also significant for the development of next-generation luminophores that both crystals containing CH_2Cl_2 and those without any crystal solvent emit NIR luminescence, as luminescence in the NIR II window is available for *in vivo* bioimaging in deeper regions.[12] Furthermore, it should be noted that the NIR emission wavelength can be modulated by changing the Pt–Pt interaction sensitive to stimuli for the environment, ancillary ligands such as Cl^- and CN^-, and the number and kind of small molecules in the crystal.

Data availability

The data that support the findings of this manuscript are openly available in *ChemSusChem*., 2023, **16**, e202301174 at **https://doi.org/10.1002/cssc.202301174** (section 1), *J. Phys. Chem. B*, 2021, **125**, 9260–9267 at **https://doi.org/10.1021/acs.jpcb.1c03753** (section 2), *Dalton Trans.*, 2022, **51**, 7068–7075 at **https://doi.org/10.1039/d2dt00368f**, *Dalton Trans.*, 2022, **51**, 1474–1480 at **https://doi.org/10.1039/D1DT03666A** (section 3), and *Dalton Trans.*, 2022, **51**, 15830–15841 at **https://doi.org/10.1039/D2DT02360A** (section 4).

Conflicts of interest

There are no conflicts to declare.

Acknowledgements

The author acknowledges Dr S. Hattori for assisting with the experimental work and helpful discussion. This work was supported by JSPS KAKENHI (No. JP21K14647).

References

1 (*a*) A. Zamora, G. Vigueras, V. Rodríguez, M. D. Santana and J. Ruiz, *Coord. Chem. Rev.*, 2018, **360**, 34–76; (*b*) X. Li, J. Wu, L. Wang, C. He, L. Chen, Y. Jiao and C. Duan, *Angew. Chem., Int. Ed.*, 2020, **59**, 6420–6427; (*c*) Y. Wu, S. Li,

Y. Chen, W. He and Z. Guo, *Chem. Sci.*, 2022, **13**, 5085–5106.

2 (*a*) S. Wan and W. Lu, *Angew. Chem., Int. Ed.*, 2017, **56**, 1784–1788; (*b*) S. Wan, J. Lin, H. Su, J. Dai and W. Lu, *Chem. Commun.*, 2018, **54**, 3907–3910.

3 (*a*) Y. Hayashi, S. Kita, B. S. Brunschwig and E. Fujita, *J. Am. Chem. Soc.*, 2003, **125**, 11976–11987; (*b*) D. H. Gibson, X. Yin, H. He and M. S. Mashuta, *Organometallics*, 2003, **22**, 337–346; (*c*) D. H. Gibson and X. Yin, *Chem. Commun.*, 1999, 1411–1412.

4 (*a*) O. S. Wenger, *Chem. Rev.*, 2013, **113**, 3686–3733; (*b*) M. J. Bryant, J. M. Skelton, L. E. Hatcher, C. Stubbs, E. Madrid, A. R. Pallipurath, L. H. Thomas, C. H. Woodall, J. Christensen, S. Fuertes, T. P. Robinson, C. M. Beavers, S. J. Teat, M. R. Warren, F. Pradaux-Caggiano, A. Walsh, F. Marken, D. R. Carbery, S. C. Parker, N. B. McKeown, R. Malpass-Evans, M. Carta and P. R. Raithby, *Nat. Commun.*, 2017, **8**, 1800; (*c*) E. Li, K. Jie, M. Liu, X. Sheng, W. Zhu and F. Huang, *Chem. Soc. Rev.*, 2020, **49**, 1517–1544.

5 (*a*) M. J. Bryant, S. Fuertes, L. E. Hatcher, L. H. Thomas and P. R. Raithby, *Faraday Discuss.*, 2023, **244**, 411–433; (*b*) B. Li, Y. Li, M. H.-Y. Chan and V. W.-W. Yam, *J. Am. Chem. Soc.*, 2021, **143**(51), 21676–21684; (*c*) P. Yu, D. Peng, L.-H. He, J.-L. Chen, J.-Y. Wang, S.-J. Liu and H.-R. Wen, *Inorg. Chem.*, 2022, **61**, 254–264; (*d*) P. Jia, X. He, J. Yang, X. Sun, T. Bu, Y. Zhuang and L. Wang, *Sens. Actuators, B*, 2023, **374**, 132803; (*e*) K. M. Fürpaß, L. M. Peschel, J. A. Schachner, S. M. Borisov, H. Krenn, F. Belaj and N. C. Mösch-Zanetti, *Angew. Chem., Int. Ed.*, 2021, **60**, 13401–13404.

6 H. Mita, H. Shingo, T. Sasaki, S. Takamizawa and K. Shinozaki, *ChemSusChem*, 2023, **16**, e202301174.

7 S. Hattori, S. Hirata and K. Shinozaki, *J. Phys. Chem. B*, 2021, **125**, 9260–9267.

8 (*a*) S. Hattori, M. Kondo, A. Sekine and K. Shinozaki, *Dalton Trans.*, 2022, **51**, 7068–7075; (*b*) S. Hattori, T. Nagai, A. Sekine, T. Otsuka and K. Shinozaki, *Dalton Trans.*, 2022, **51**, 1474–1480.

9 S. Hattori, T. Nakano, N. Kobayashi, Y. Konno, E. Nishibori, T. Galica and K. Shinozaki, *Dalton Trans.*, 2022, **51**, 15830–15841.

10 (*a*) V. K. Soni, H. S. Hwang, Y. K. Moon, S.-W. Park, Y. You and E. J. Cho, *J. Am. Chem. Soc.*, 2019, **141**, 10538–10545; (*b*) D. Cambié, C. Bottecchia, N. J. W. Straathof, V. Hessel and T. Noël, *Chem. Rev.*, 2016, **116**, 10276–10341; (*c*) C. K. Prier, D. A. Rankic and D. W. C. MacMillan, *Chem. Rev.*, 2013, **113**, 5322–5363.

11 (*a*) M. Martínez-Alonso, C. G. Jones, J. D. Shipp, D. Chekulaev, H. E. Bryant and J. A. Weinstein, *J. Biol. Inorg. Chem.*, 2024, **29**, 113–125; (*b*) R. E. Doherty, I. V. Sazanovich, L. K. McKenzie, A. S. Stasheuski, R. Coyle, E. Baggaley, S. Bottomley, J. A. Weinstein and H. E. Bryant, *Sci. Rep.*, 2016, **6**, 22668.

12 (*a*) I. Melendo, S. Fuertes, A. Martín and V. Sicilia, *Inorg. Chem.*, 2024, **63**, 5470–5480; (*b*) R. J. Salthouse, P. Pander, D. S. Yufit, F. B. Dias and J. A. G. Williams, *Chem. Sci.*, 2022, **13**, 13600–13610; (*c*) H. J. Park, C. L. Boelke, P. H.-Y. Cheong and D.-H. Hwang, *Inorg. Chem.*, 2022, **61**, 5178–5183; (*d*) T. Li, C. Li, Z. Ruan, P. Xu, X. Yang and P. Yuan, *ACS Nano*, 2019, **13**, 3691–3702; (*e*) C. Li, G. Chen, Y. Zhang, F. Wu and Q. Wang, *J. Am. Chem. Soc.*, 2020, **142**, 14789–14804; (*f*) Y. Sun, F. Ding, Z. Zhou, C. Li, M. Pu, Y. Xu, Y. Zhan, X. Lu, H. Li, G. Yang, Y. Sun and P. J. Stang, *Proc. Natl. Acad. Sci. U. S. A.*, 2019, **116**, 1968–1973.

